Niche homeostasis in multi-lineage stem cell populations is maintained through intercellular redox gradients

Olivia Majhi[1], Aishwarya Chhatre[1], Tanvi Chaudhary[1] and Devanjan Sinha[1#]

[1]Department of Zoology, Institute of Science, Banaras Hindu University, Varanasi, Uttar Pradesh, India

[#]To whom correspondence should be addressed:

Address for correspondence:
Dr. Devanjan Sinha,
Department of Zoology,
Institute of Science,
Banaras Hindu University,
Varanasi – 221005,
Uttar Pradesh, India
India
Email: devanjan@bhu.ac.in

Summary

Reactive oxygen species (ROS), predominantly derived from mitochondrial respiratory complexes, have evolved as key molecule influencing cell fate decisions. In stem cells, differential ROS thresholds serve as maintenance or pro-differentiation functions. Although these redox-dependent events are mainly cell intrinsic in nature, our observations indicate involvement of these oxygen-derived entities as intercellular communicating agents. In multi-lineage *Drosophila* germline, neighbouring GSCs and CySCs maintain differential redox thresholds where CySCs by virtue of their higher redox-state regulate physiological ROS levels of germline. Disruption of the intercellular redox equilibrium between the two adjoining stem cell populations resulted in deregulated niche architecture and loss of GSCs, which was mainly attributed to loss of contact based signalling and uncontrolled CySC proliferation. Our observations hint towards crucial role of intercellular redox gradients originating from somatic progenitors, CySCs in niche homeostasis and non-autonomous maintenance of germline immortality.

Highlights:

- CySCs maintain higher ROS threshold than GSCs
- Existence of intercellular redox gradients between stem cell populations in the niche
- Redox-dependent maintenance of GSC fate by CySCs

Introduction

Studies from the past few decades have shown the apparent role of Reactive Oxygen Species (ROS) in regulation of cell signalling events influencing various biological processes involving metabolism, gene expression, immune responses, protein translation, and protein-protein interactions[1, 2]. ROS is mainly generated as a consequence of metabolic processes and comprises of superoxides, hydrogen peroxides as the major signalling intermediates[3]. Generally, the sources of ROS are compartmentalized in co-occurrence with their targets causing atomic level modifications, thus making these oxygen species important signalling mediators[4]. For example, mitochondria, a major source of superoxide and dismutated peroxides under physiological conditions[5, 6], are shown to localize dynamically towards nucleus, effecting oxidation induced hypoxic response and instigating DNA alterations that subsequently reshape gene expression profiles[7]. Localized ROS production contributed by NADH oxidases are distributed across different cellular regions[8]. Intracellular hydrogen peroxide gradients maintained by thioredoxin system allow intercompartmental exchanges among different cellular regions including the endoplasmic reticulum (ER), mitochondria and peroxisomes[9-11].

The process of redox relays is conserved, connected to various cell fate decisions, and play a fundamental role in self-renewal, differentiation of stem cell populations [12]. Stem cells whether embryonic or adult including hematopoietic stem cells (HSCs), neural stem cells (NSCs), mesenchymal stem cells (MSCs) and germinal stem cells (GSCs) maintain a low redox profile, characterized by subdued mitochondrial respiration, accumulated glycolytic and pentose phosphate pathway intermediates[13-17]. Levels of ROS are tightly regulated and elevated amounts promotes early differentiation and atypical stem cell behaviour[18]. However, leading evidences suggest that many transcription factors require oxidative environment for maintenance of pluripotent states. For instance, physiological ROS levels play a crucial role in genome maintenance of embryonic stem cells[13]. Multipotent hematopoietic progenitors require relatively high baseline redox state for their maintenance and self-renewal[16, 19]. NSCs self-renew and proliferate through Nox2

dependent activation of Akt pathway[14]. Suppression of Nox system or mitochondrial ROS compromises the maintenance of these self-renewing populations and promote their differentiation or death[18]. These evidences point towards essentially of a perfectly tuned redox state for balancing the pluripotent and differentiated states. However, it is not very clear, how the stem cells harmonize their redox potential by possessing a restrained oxidant system.

To address this fundamental question, we studied the role of ROS in multi-stem cell lineage-based niche architecture in *Drosophila* testis. The testicular stem cell niche is composed of a central cluster of somatic cells called the hub which contacts eight to eleven GSCs arranged in a round array[20, 21]. A pair of cystic stem cells (CySCs) originating the somatic lineage cyst cells, enclose each GSC and make their own independent connections with the hub and GSCs via adherens junctions[22-26]. The hub cells secrete Unpaired family of cytokines that defines niche occupancy and self-renewal of both GSCs and CySCs through Jak-Stat signalling[27, 28]. CySCs also repress GSC differentiation by effecting Bone morphogenetic protein (BMP) response that suppress transcription of bag-of-marbles (Bam)[29, 30]. The GSCs divide asymmetrically to form gonialblast that get surrounded by two CySC daughters, progenitors of cyst cells. Concerted asymmetric division of both GSC and CySC is essential for proper cyst formation[31]. A developing cyst contains a dividing and differentiating gonialblast encircled by cyst cells that provide nourishment to developing spermatids[32, 33]. Both GSCs and CySCs coordinate their growth through a plethora of growth factor signal transductions[31], but the maintenance of GSCs and their differentiation in the spatially controlled microenvironment is still not very clear.

We found the existence of a redox differential between the two stem cell populations important for niche homeostasis. In addition to morphogenetic signals, somatic lineage CySCs play a prime role in defining niche architecture through redox dependent processes and maintaining physiological ROS levels in GSCs. CySC mitochondria cluster in GSC-CySC boundary that correlate with an oxidant peak at the interface, diffusing into the GSCs. This non-autonomous regulation of GSC redox state by CySC becomes evident through disruption of the intercellular ROS equilibrium between these two interlacing populations. Depletion of Sod1 in CySCs results in disruption of

niche composition and elevated ROS in GSCs, causing their early differentiation. Elevation of the antioxidant system in the progenitors promoted self-renewal and maintenance of the germline, and repressed precocious differentiation. Redox imbalance induced niche disequilibrium was apparent through uncontrolled CySC/cyst cell proliferation due to autonomous activation of ROS induced pro-proliferative transductions and loss of cell-cell contact signalling. Our results in multi-stem cell lineage-based germline system indicate a dual role of ROS where a higher redox state in somatic CySCs not only maintains its self-renewing processes but non-autonomously diffuses into GSC at physiological levels to foster its maintenance.

Results

Redox state of GSC is maintained by asymmetric distribution of CySC mitochondria

The apical region of the *Drosophila* testis incorporates a cluster of differentiated cells the hub, surrounded by GSCs in a rosette arrangement with one GSC being enclosed by two CySCs (Fig. 1A). In control flies (*Tj-Gal4* crossed with *OregonR*$^{+}$ progeny), both the cell types presented contrasting morphology of mitochondria upon complex V-specific ATP5A staining, where the organelle were more fragmented in Vasa^{+} GSCs as compared to Traffic jam (Tj)$^{+}$ CySCs which showed a more fused organization (Fig. 1B#, C, D). Profiling of mitochondrial distribution showed higher propensity of ATP5A overlap with Tj, indicating CySCs to be more mitochondria dense compared to GSC (Fig. 1F). The CySC mitochondria were found to be primarily clustered near the GSC-CySC boundary as illustrated by intensity profile (Fig. S1A'") and sectioning through X-Z and Y-Z clipped plane (Fig. S1B-B'). The ATP5A labelling overlapped with *TFAM-GFP*, a mitochondrial transcription factor involved in its DNA maintenance[34], further confirming the mitochondrial patterning observed between these two stem cell populations (Fig. S1C'). The centering of mitochondria near the GSC-CySC boundary, together with its contrasting dispersion, was found to be associated with variance in the intensity of ROS reporter line *gstD1-GFP* [35] at the niche zone (Fig. 1H and S1D-D'). The redox gradient was found to peak at the Tj-Vasa boundary which gradually diffused into Vasa^{+} GSCs suggesting establishment of GSC redox state through

CySCs (Fig. 1Q). Generation of GSC intrinsic oxidative environment would have resulted in constant continuum of *gstD1*-GFP intensity across the Vasa-stained structure. The presence higher ROS gradient at the GSC-CySC interface was also determined by 2D-Plot profile of Vasa, Tj and *gstD1*-GFP across the different cell types (Fig. S1E).

To further demonstrate the CySC induced redox state in GSC maintenance and differentiation, we depleted the expression of superoxide dismutase 1 (Sod1) in CySCs and early differentiating cyst cells using *Tj-Gal4* (*Tj>Sod1i*) driver line. The elevation of ROS at the apical tip of the testis was validated using overall *gstD1*-GFP (Fig. 1K, P and R) and DHE fluorescence (Fig. S1F). Higher CySC redox state resulted in corresponding increase in GSC ROS profile as indicated by a greater degree of Vasa-GFP (V∩G) intersection compared to control, suggesting non-autonomous maintenance of GSC redox gradient by CySCs (Fig. 1Q). The surge in ROS levels of GSCs upon lowering of antioxidant defences in CySCs, was additionally confirmed through enhanced Vasa:*gstD1*-GFP colocalization intensities in *Sod1i* populations (MCC^{mean} = 0.482) with respect of controls (MCC^{mean} = 0.276) (Fig. 1S). In summary, our results indicate that CySCs by virtue of their clustered mitochondria polarized towards GSCs elevate the cellular ROS gradient at the interface between two stem cell populations which in turn non-autonomously maintains the physiological redox status of the germline.

Balanced CySC redox profile is crucial for its proliferation and GSC maintenance

High ROS in *Tj>Sod1i* showed a striking increase in $DAPI^+$ nuclei in the tip of testis (Fig. 1G and L). The overcrowding of the $DAPI^+$ nuclei was mainly attributed to an increase in Tj^+ CySCs and early differentiating cyst cells, number which was found to be almost double to that of control (Fig. 2A', B' and E). The $Zfh1^+$ cells that specifically stains the CySCs was also found be to ~2-fold higher (Fig. 2F). $Vasa^+$ cells flanking the hub however, substantially reduced in number (Fig. 2C'-D'' and G), which was validated through lower detectable levels of Vasa even when its expression per cell remained unchanged (Fig. S2O). The data was further verified using *Sod1i* localized

in different chromosome to avoid any chromosome or balancer-based biasness (Fig. S1G-L). However, the phenotypic effect of higher ROS was limited to its origin in CySCs only because ablation of GSC redox status did not cause any marked change in niche composition. *Nos-Gal4* driven knock-down of Sod1 in GSCs did not result in significant change in CySC number (Fig. S2A', B' and E) but effected a considerable reduction on Vasa^{+} GSCs (Fig. S2C', D' and F), aligning with previous observations[17]. Although, Sod1 is the predominant enzyme which also localizes in the intermembrane space of mitochondria, we observed a similar result upon depleting the matrix localized Sod2 in both GSCs and CySCs (Fig. S2G- S2M) indicating involvement of mitochondrial ROS for the observed cellular phenotypes.

To confirm active proliferation of cells and rule out the possibility of arrested growth, we utilized fly- Fluorescent Ubiquitination-based Cell Cycle Indicator (FUCCI) system which comprises of two reporter constructs marking G1/S transition (green), S (red) and G2/early mitosis (yellow) (Fig. 2H)[36]. *Tj>Sod1i* testes presented a ~2-fold increase in cell number across all stages of cell-cycle (Fig 2I). The enhanced number of dividing cells was contributed mainly by progressive division of CySCs, showing >2-fold difference in accumulation of Zfh1^{+} nuclei in S and G2/M phases (Fig. 2N-Q, U-X and J). The number of Zfh1 labelled cells in G1/S transition was also substantially more (Fig. 2M and T), indicating dysregulated redox ensued increased mitotic index of CySCs. Downregulation of Sod1 in GSCs through *Nos-Gal4* demonstrated no significant change in G1/S, S and G2/M phase numbers, confirming our previous observation that altering ROS levels in GSCs does not have any non-autonomous effect on CySCs (Fig. S2N).

CySC induced ROS couples precocious differentiation of stem cell lineages

Since, Tj^{+} foci which stains nuclei of both CySCs and early differentiating cells[37] was elevated and number of dividing CySC-specific Zfh1^{+} cells were less than the total count (Fig. 2I and J), we labelled *Tj>Sod1i* testes with Zfh1 and differentiation marker Eya (Eyes absent) which reflected higher number of Eya^{+} cells (Fig. 3A, B, and D) located much closer to the hub than controls (Fig. S3E). Premature expression of the differentiation marker resulted in a population of differentiating cyst precursor cells co-

presenting Eya-Zfh1 (Fig. 3A", B" and D), which significantly deviated from normal partitioning of representative populations (Fig. 3C). No change in arrangement of Zfh1$^+$ and Eya$^+$ cells was observed in *Nos>Sod1i* testis (Fig. S3A-D).

However, inflated redox condition in GSCs gained non-autonomously from CySCs, affected its number and differentiation state. Together with reduction in Vasa$^+$ cells shown earlier (Fig. 2G), we detected spermatogonia expressing differentiation-promoting factor Bam to be much closer to the hub in *Tj>Sod1i* testes (Fig. 3E" and F") with the mean distance between hub and Bam$^+$ zone shortened by ~7 microns (Fig 3G). The relative advancement of spermatogonial differentiation towards the hub was also ascertained by tracking the transformation of GSC-specific spectrosome into branched fusomes connecting the multi-cell gonialblast (Fig. 1A). The branching fusomes were found more proximal to hub than controls (Fig. 3H, I" and J"), along with parallel reduction in number of spectrosomes, implying a decline in early-stage germ cells (Fig. S3F). The loss could possibly be attributed to a higher oxidizing environment in GSCs and loss of intercellular contacts, particularly with hub cells (Fig. 2C# and D#). The observation corroborated with decreased expression pattern of E-cadherin in *Tj>Sod1i* (Fig. S3G), which was almost negligible near the hub (Fig. 3K-M) and hence, could possibly be one of the major reasons for GSC dissociating from the hub (Fig. 2D#) and differentiating due to absence of self-renewing signals. Indeed, disengagement of GSCs from the hub caused reduction in Socs36E and Ptp61F transcripts those are transcriptionally activated by maintenance factor STAT and act as drivers of E-cadherin expression (Fig. 3N and 3O).

Altered CySC ROS affects EGFR response

Ligands secreted by GSCs tigger downstream components of EGFR in CySCs that results differences in cell polarity and segregates self-renewing from differentiating populations[38]. Loss of inter-cell communication compromised this regulation resulting *Tj>Sod1i* cells to show lower levels of cell-polarity marker Dlg (Fig. 4A", B" and C), leading to accumulation of unregulated differentiating population of cyst cells with reduced polarity (Fig. 4D). Since, Dlg expression is dependent on EGFR[39], impairment in its reception was reflected in net reduction in pErk levels across sections

in *Sod1i* testis (Fig. 4E). However, this reduction was mainly limited to regions surrounding the hub, among CySC populations (Fig. 4F and G''-H''), thereby affecting their maintenance. Cyst cells presented relatively higher levels of pErk expression, relating to its established role in promoting differentiation (Fig. 4F, G'-H'). In *Tj>Sod1i* tissues, the area labelled with pErk was found to be significantly expanded (Fig. 4I) and located comparatively closure to the hub (Fig. 4J), supporting unrestrained division and premature differentiation of early cyst cells under high redox conditions.

Premature CySCs differentiation is promoted by activated PI3K/Tor signalling

PI3K/Tor signalling is essential for proper CySCs self-renewal and differentiation with lower levels of its reporter p4E-BP at Tj^+ regions closer to the hub and higher expression in distant differentiating zones[40]. But in *Tj>Sod1i*, the overall levels of p4E-BP were noticeably higher (Fig. 5A''', B''' and C) which got extended to areas neighbouring the hub (Fig. 5A and B). Activation of PI3K also caused Akt-dependent G1/S transition through Cyclin-D accumulation whose transcript levels were found higher in *Sod1i* testis (Fig. 5D and E). Thus, it is conceivable that ROS-mediated CySCs differentiation and proliferation might be due to activated PI3K/Tor. The idea was supported by suppression of CySC proliferation by downregulating PI3K/Tor using a single copy of $PI3K^{DN}$ (dominant-negative allele) in Tj-expressing cells. Reduced dosage of PI3K actively abolished *Sod1i* mediated over-proliferation of CySCs (Fig. 5F, I'' and J'') and partially rescued the number of GSCs (Fig. 5G, L' and M'), highlighting the importance of a balanced ROS for optimising the activation of maintenance factors.

Discussion:

ROS is a crucial mediator of stem cell maintenance where these species act as second messengers to induce different post-translational protein modifications thereby,

affecting cell fate[41, 42]. Effectuation of ROS is mainly considered to be autocrine in nature where generation of these oxidative species is compartmentalized with their site of action. Recent studies have reported non-autonomous generation of ROS by NOX enzymes or upon stimulation by growth factors, to play a critical role in regenerative growth[43-45]. However, in either of the cases, the target cell serves as the source and consequent response.

Our observations in multi-lineage *Drosophila* germinal stem cell niche suggested a previously unaccounted transmission of redox signals inter-cellularly that act as an organizer of niche homoeostasis. Both the stem cell populations, GSCs and CySCs maintain differential levels of ROS that can be attributed to variations in the mitochondrial distribution. CySCs exhibit a predominance of interconnected mitochondrial networks oriented towards the germ-cell primordia, whereas GSCs display a higher prevalence of fragmented mitochondrial structures, that resulted in accumulation of ROS predominantly at CySC-GSC interface. The higher ROS threshold of CySCs and resultant CySC-GSC oxidative gradient maintained the physiological redox state of GSC, exerting a localized regulatory influence. High CySC ROS due to impairment of antioxidant defence promoted GSCs to differentiate which was also reflected when GSC ROS was elevated. However, altered GSC ROS did not have any significant effect on CySC populations.

The GSCs by virtue of their attachment with the hub cells via adherens junction, receive the maintenance signal, Upd that trigger the JAK-STAT pathway[27, 28]. Suppression of STAT lead to activation of differentiation transcription factor Bam which is typically expressed in four, eight and early sixteen-cell stages of the spermatogonial cyst, acting as a switch from transit amplifying cells to spermatocyte differentiation[46, 47]. Normally, GSC differentiation is associated with downregulation of E-cadherin, which serves as a quality control mechanism, ensuring that only undifferentiated and functional stem cells persist within the niche, while differentiating GSCs lose the competition for niche occupancy and are compelled to vacate[25]. Studies have shown ROS effected S-glutathionylation of STAT impaired its phosphorylation by JAK and inhibited its transcriptional activity[48, 49]. We found reduced presence of STAT dependent transcripts, Socs36E and E-cadherin under high CySC ROS status,

causing lower E-cadherin levels that resulted in detachment of GSCs from the hub, consistent with previous findings demonstrating downregulation of E-Cadherin in primordial germline due to increased ROS levels[50-53] and further confirming our idea on the existence of intercellular redox balance between CySCs and neighbouring GSCs.

In contrast to GSCs, ROS imbalance in CySCs demonstrated a growth promoting function, along with induction of accelerated differentiation. The increased proliferation of CySCs was mainly attributed to deregulation of PI3K/Tor and EGFR signalling. Loss of CySC-GSC communication under higher redox state, was also reflected through lower EGFR response in vicinity of the hub. EGFR signalling originate from germline and act on the neighbouring soma, influencing each other's cellular destinies. GSCs secrete EGFR ligands, which bind to corresponding receptors present on neighbouring cyst cells to activate the downstream components of the cascade and play a pivotal role in deciding the cell fate[54, 55]. In fact, EGFR play a crucial role in maintenance of cell-polarity that segregates self-renewing CySC populations from the ones receiving differentiation cues[38]. Compromised EGFR reception disrupted this polarity leading to accumulation of CySC/cyst cells co-expressing both stemness and differentiation markers. Among the precociously differentiating populations both EGFR effector and ROS was found to be high which agrees with previous studies on ROS-mediated activation of EGFR in promoting differentiation. The observations show that fine-tuning of CySC redox homeostasis is critical for niche composition by balancing the two inter-communicating stem cell populations.

Even though, our study focuses on ROS signals originating from CySCs, we do not rule out the possibilities of hub cells playing an equivalent role in maintaining GSC populations, given their parallel effect in suppressing GSC differentiation[28]. We had tried using E-132 driver to express *Sod1i* lines in hub cells but were challenged by substantial adverse effect on fly viability. We also avoided usage of Gal80 dependent clonal populations and maintained a homogenous genetic background, to prevent false readouts due to diffusion of ROS signals in unaltered neighbourhood.

The proposed concept of intercellular communication through ROS signals extends beyond *Drosophila* germline and might be of importance in deciphering the

biochemical adaptability and plasticity of different niches influencing stem cell state and fate. ROS may be one among the spectrum of cues that ensures niche size and architecture by coupling division among the neighbours to prevent stem cell loss and aging. This has been observed in neural stem cells where inflammation-induced quiescence is one of the ways to recover the regenerating capacity of the aging brain[56]. In additional to metabolic variations, the dependence of the germline on the adjacent somatic neighbours for its redox state might be one the reasons behind its presumed immortal nature and renitence to aging[57]. The same can also be applied to cancer stem cells which maintain niche occupancy and resist oxidative stress induced apoptosis by probably, receiving redox cues from the environment.

Limitations of the study

Although our study establishes non-cell autonomous nature of ROS signalling, a comprehensive understanding of the specific role played by paracrine redox in modulating regulatory pathways such as JAK-STAT, EGFR and PI3K/Tor balancing stemness/differentiation and maintaining the overall niche composition, needs further attention. Further work is also required to elucidate the driver mechanisms that tune the oxidative state of the surrounding somatic populations for niche plasticity.

Experimental Procedures

Fly strains

Fly stocks were maintained and crosses were set at 25 °C on normal corn meal and yeast medium unless otherwise indicated. All fly stocks (BL-24493) *UAS SOD1 RNAi*, (BL-32909) *UAS SOD1 RNAi*, (BL-29389) *UAS SOD1 RNAi*, (BL-32983) *UAS SOD2*

RNAi, (BL-8288) *UAS PI3K^{DN}*, (BL- 25751) *UAS Dcr-nos*, (BL-55122) *UAS-FUCCI*, were obtained from Bloomington Drosophila Stock Centre. *Nos-Gal4*, *Tj-Gal4*, *Tj-Gal4-BamGFP*, *gstD1-GFP*, *TFAM-GFP* were kind gift from U. Nongthomba, P. Majumder, K. Ray, B. C. Mandal, Hong Xu labs respectively. For optimal Gal4 activity parent crosses were shifted to 29 °C till the eclosion of adults. 3-5 days old males were taken for all the experiments. The control lines for all experiments are the corresponding Gal4-line crossed with wild type *OregonR^{+}*.

Dissection and immunostaining

Anesthetized flies were dissected in 1X Phosphate Buffer Saline (PBS). All incubations were carried out at room temperature (25 °C) unless otherwise mentioned. Testes were fixed in 4% paraformaldehyde for 30 minutes, followed by multiple washes with 0.1% PBTX (PBS + TritonX 100). Post-blocking in 0.5% Bovine Serum Albumin, testis was incubated overnight at 4°C for primary antisera, followed by washing in 0.1% PBTX 3 times 15 minutes each before incubating with secondary antibody. The tissues were counterstained with DAPI (4,6-diamidino-2-phenylindole) for 20 minutes, followed by three washes in 0.1% PBTX 10 minutes each. The dpErk was labelled by dissecting fly testes in Schneider's media, followed by fixation in 4% PFA for 30 min, 3x wash in 0.1% PBTX, blocked and incubated in primary antibody overnight; each step supplemented with phosphatase inhibitor cocktail 2 (1:100, Sigma, cat#P5726). Samples were mounted in DABCO anti-fade medium prior imaging.

The following primary antibodies were used in the experiments - anti-FasIII (7G10) (1:120, DSHB (Developmental Studies Hybridoma Bank)), anti-Eya (1:50, DSHB), anti-DEcad (DCAD2) (1:50, DSHB), anti-α-Spectrin (3A9) (1:20, DSHB), anti-βtubulin (1:300, DSHB), anti-pERK (1:100, Cell Signaling (4370)), ATP5A (1:700, Abcam (ab14748)), anti-Tj (1:5000), anti-Vasa (1:4000), anti-Zfh1(1:2000). The primary labelling was detected using appropriate Alexa-Flour tagged secondary antibody (ThermoFisher Scientific).

To assess superoxide levels, testes were dissected in Schneider's medium (SM) and immediately incubated in 30μM Dihydroxyethidium (DHE) at 25 °C in dark. Testes were

washed thrice with SM for 7 minutes each before quantifying the emitted fluorescence using SpectraMax iD5 (Molecular Devices).

Quantitative Reverse transcription–PCR

For semi-quantitative RT-PCR and qRT-PCR analyses, total RNA was isolated from testes of 3-5 days old male flies using Qiagen RNA extraction kit. RNA pellets were resuspended in nuclease-free water and quantity of RNA was spectrophotometrically estimated. First strand cDNA was synthesized from 1-2 µg of total RNA as described earlier. The prepared cDNAs were subjected to real time PCR using forward and reverse primer pairs as listed below, using 5 µl qPCR Master Mix (SYBR Green, ThermoFisher Scientific), 2 pmol/µl of each primer per reaction for 10 µl final volume in ABI 7500 Real time PCR machine. The fold change in expression was calculated through $2^{-\Delta\Delta Ct}$ method.

Imaging and image analysis

Confocal imaging was carried out using Zeiss LSM 900 confocal microscope, using appropriate dichroics and filters. Images were further analyzed and processed for brightness and contrast adjustments using ImageJ (Fiji). Mean intensity measurements were carried out using standard Fiji plug-ins, 2D surface plot quantification or Zeiss Zen software as indicated. Quantification of cell number/nuclei in single or co-stained populations (Tj, Vasa, Zfh1, Eya, FUCCI) were performed from individual slices of z-stacks using semi-automated Cell Counter plugin in Fiji for all the mentioned genotypes. The relative distance from the two reference points in the images was estimated through Inter-edge Distance ImageJ Macro v2.0 from Github. All images were assembled using Adobe Photoshop version 21.2.1.

Immunoblot Analysis

Protein was extracted from the dissected testes using RIPA buffer as described previously and quantified using Bradford reagent (Biorad). Equivalent concentration of lysate was denatured using 1X Laemelli Buffer with 1 M DTT at 95°C, separated in

10% SDS-PAGE and transferred onto PVDF membranes. Membranes were blocked with commercial blocking solution in TBST base before sequential primary antibody incubation with anti-Vasa and anti-β-Tubulin (DSHB, E7). Secondary detection was performed using HRP-tag anti-mouse antibody (GE Amersham).

Statistical analyses

All data points represent at least three biological replicates and the sample sizes carrying adequate statistical power are mentioned in the figure legends. Statistical significance for each experiment were calculated using two tailed Student's t-test unless otherwise mentioned, using GraphPad Prism 8 software. The P values were calculated through pairwise comparison of the data with wild type or driver alone and driven RNAi lines. Significance values for sample sizes mentioned in figure legends were represented as *P < 0.01, **P <0.001, or ***P < 0.0001.

Author contribution

D.S. and O.M conceived the study and designed the experiments. O.M, A.C and T.C performed the experiments. D.S and O.M analyzed the data and wrote the manuscript.

Acknowledgements

We thank P. Majumder, U. Nongthomba, K. Ray, G. Ratnaparkhi, B. C. Mandal, Hong Xu lab and S. C. Lakhotia for kindly sharing some of the transgenic fly lines. Christian Bökel for sharing experimental protocols. Anti-Tj antibody was a generous gift from Prof. D. Godt, University of Toronto. Anti-Vasa and Anti-Zfh1 were kindly gifted by Prof. R. Lehmann, New York University. We also thank Dr. Bama Charan Mandal for generously sharing his Confocal microscope imaging system and Sudeshna Majumder for preliminary data. We acknowledge BDSC for fly stocks and DSHB for antibodies. This work is supported by Innovative Young Biotechnologist Award by Department of Biotechnology (BT/12/IYBA/2019/01), Early Career Research Award by Science and Engineering Research Board (ECR/2018/000009), BHU-Institute of Eminence grant (R/Dev/IoE/Incentive/2021-22/32452). The authors also acknowledge

financial support from DST-INSPIRE fellowship (to O.M.), UGC-CAS doctoral fellowship (to T.C.).

Declaration of interest

The authors declare no competing interests

Lead contact

Further information and requests for resource and reagents should be directed and will be fulfilled by Devanjan Sinha (devanjan@bhu.ac.in).

Materials Availability

This study did not generate any new reagents or tools.

Data and code availability

The lead contact will share all raw data associated with this paper upon request. This study did not utilize or generate any unique datasets or codes.

References

1. Holmstrom, K.M. and T. Finkel, *Cellular mechanisms and physiological consequences of redox-dependent signalling.* Nat Rev Mol Cell Biol, 2014. **15**(6): p. 411-21.
2. D'Autreaux, B. and M.B. Toledano, *ROS as signalling molecules: mechanisms that generate specificity in ROS homeostasis.* Nat Rev Mol Cell Biol, 2007. **8**(10): p. 813-24.
3. Schieber, M. and N.S. Chandel, *ROS function in redox signaling and oxidative stress.* Curr Biol, 2014. **24**(10): p. R453-62.
4. Maryanovich, M. and A. Gross, *A ROS rheostat for cell fate regulation.* Trends Cell Biol, 2013. **23**(3): p. 129-34.
5. Murphy, M.P., *How mitochondria produce reactive oxygen species.* Biochem J, 2009. **417**(1): p. 1-13.
6. Hamanaka, R.B. and N.S. Chandel, *Mitochondrial reactive oxygen species regulate cellular signaling and dictate biological outcomes.* Trends Biochem Sci, 2010. **35**(9): p. 505-13.
7. Al-Mehdi, A.B., et al., *Perinuclear mitochondrial clustering creates an oxidant-rich nuclear domain required for hypoxia-induced transcription.* Sci Signal, 2012. **5**(231): p. ra47.

8. Bedard, K. and K.H. Krause, *The NOX family of ROS-generating NADPH oxidases: physiology and pathophysiology.* Physiol Rev, 2007. **87**(1): p. 245-313.
9. Appenzeller-Herzog, C., et al., *Transit of H2O2 across the endoplasmic reticulum membrane is not sluggish.* Free Radic Biol Med, 2016. **94**: p. 157-60.
10. Mishina, N.M., et al., *Which Antioxidant System Shapes Intracellular H(2)O(2) Gradients?* Antioxid Redox Signal, 2019. **31**(9): p. 664-670.
11. Yoboue, E.D., R. Sitia, and T. Simmen, *Redox crosstalk at endoplasmic reticulum (ER) membrane contact sites (MCS) uses toxic waste to deliver messages.* Cell Death Dis, 2018. **9**(3): p. 331.
12. Rehman, J., *Empowering self-renewal and differentiation: the role of mitochondria in stem cells.* J Mol Med (Berl), 2010. **88**(10): p. 981-6.
13. Li, T.S. and E. Marban, *Physiological levels of reactive oxygen species are required to maintain genomic stability in stem cells.* Stem Cells, 2010. **28**(7): p. 1178-85.
14. Le Belle, J.E., et al., *Proliferative neural stem cells have high endogenous ROS levels that regulate self-renewal and neurogenesis in a PI3K/Akt-dependant manner.* Cell Stem Cell, 2011. **8**(1): p. 59-71.
15. Chuikov, S., et al., *Prdm16 promotes stem cell maintenance in multiple tissues, partly by regulating oxidative stress.* Nat Cell Biol, 2010. **12**(10): p. 999-1006.
16. Owusu-Ansah, E. and U. Banerjee, *Reactive oxygen species prime Drosophila haematopoietic progenitors for differentiation.* Nature, 2009. **461**(7263): p. 537-41.
17. Tan, S.W.S., et al., *Redox Homeostasis Plays Important Roles in the Maintenance of the Drosophila Testis Germline Stem Cells.* Stem Cell Reports, 2017. **9**(1): p. 342-354.
18. Zhou, G., et al., *Optimal ROS Signaling Is Critical for Nuclear Reprogramming.* Cell Rep, 2016. **15**(5): p. 919-925.
19. Sinenko, S.A., J. Shim, and U. Banerjee, *Oxidative stress in the haematopoietic niche regulates the cellular immune response in Drosophila.* EMBO Rep, 2011. **13**(1): p. 83-9.
20. Davies, E.L. and M.T. Fuller, *Regulation of self-renewal and differentiation in adult stem cell lineages: lessons from the Drosophila male germ line.* Cold Spring Harb Symp Quant Biol, 2008. **73**: p. 137-45.
21. Hime, G.R., J.A. Brill, and M.T. Fuller, *Assembly of ring canals in the male germ line from structural components of the contractile ring.* J Cell Sci, 1996. **109 (Pt 12)**: p. 2779-88.
22. Gonczy, P. and S. DiNardo, *The germ line regulates somatic cyst cell proliferation and fate during Drosophila spermatogenesis.* Development, 1996. **122**(8): p. 2437-47.
23. Fabrizio, J.J., M. Boyle, and S. DiNardo, *A somatic role for eyes absent (eya) and sine oculis (so) in Drosophila spermatocyte development.* Dev Biol, 2003. **258**(1): p. 117-28.
24. Hardy, R.W., et al., *The germinal proliferation center in the testis of Drosophila melanogaster.* J Ultrastruct Res, 1979. **69**(2): p. 180-90.
25. Chen, S., M. Lewallen, and T. Xie, *Adhesion in the stem cell niche: biological roles and regulation.* Development, 2013. **140**(2): p. 255-65.
26. Inaba, M., et al., *E-cadherin is required for centrosome and spindle orientation in Drosophila male germline stem cells.* PLoS One, 2010. **5**(8): p. e12473.

27. Kiger, A.A., et al., *Stem cell self-renewal specified by JAK-STAT activation in response to a support cell cue.* Science, 2001. **294**(5551): p. 2542-5.
28. Tulina, N. and E. Matunis, *Control of stem cell self-renewal in Drosophila spermatogenesis by JAK-STAT signaling.* Science, 2001. **294**(5551): p. 2546-9.
29. Song, X., et al., *Bmp signals from niche cells directly repress transcription of a differentiation-promoting gene, bag of marbles, in germline stem cells in the Drosophila ovary.* Development, 2004. **131**(6): p. 1353-64.
30. Kawase, E., et al., *Gbb/Bmp signaling is essential for maintaining germline stem cells and for repressing bam transcription in the Drosophila testis.* Development, 2004. **131**(6): p. 1365-75.
31. Losick, V.P., et al., *Drosophila stem cell niches: a decade of discovery suggests a unified view of stem cell regulation.* Dev Cell, 2011. **21**(1): p. 159-71.
32. Jemc, J.C., *Somatic gonadal cells: the supporting cast for the germline.* Genesis, 2011. **49**(10): p. 753-75.
33. Zoller, R. and C. Schulz, *The Drosophila cyst stem cell lineage: Partners behind the scenes?* Spermatogenesis, 2012. **2**(3): p. 145-157.
34. Larsson, N.G., et al., *Mitochondrial transcription factor A is necessary for mtDNA maintenance and embryogenesis in mice.* Nat Genet, 1998. **18**(3): p. 231-6.
35. Sykiotis, G.P. and D. Bohmann, *Keap1/Nrf2 signaling regulates oxidative stress tolerance and lifespan in Drosophila.* Dev Cell, 2008. **14**(1): p. 76-85.
36. Zielke, N., et al., *Fly-FUCCI: A versatile tool for studying cell proliferation in complex tissues.* Cell Rep, 2014. **7**(2): p. 588-598.
37. Li, M.A., et al., *The large Maf factor Traffic Jam controls gonad morphogenesis in Drosophila.* Nat Cell Biol, 2003. **5**(11): p. 994-1000.
38. Castanieto, A., M.J. Johnston, and T.G. Nystul, *EGFR signaling promotes self-renewal through the establishment of cell polarity in Drosophila follicle stem cells.* Elife, 2014. **3**.
39. Papagiannouli, F., C.W. Berry, and M.T. Fuller, *The Dlg Module and Clathrin-Mediated Endocytosis Regulate EGFR Signaling and Cyst Cell-Germline Coordination in the Drosophila Testis.* Stem Cell Reports, 2019. **12**(5): p. 1024-1040.
40. Amoyel, M., et al., *Somatic stem cell differentiation is regulated by PI3K/Tor signaling in response to local cues.* Development, 2016. **143**(21): p. 3914-3925.
41. Sinenko, S.A., et al., *Physiological Signaling Functions of Reactive Oxygen Species in Stem Cells: From Flies to Man.* Front Cell Dev Biol, 2021. **9**: p. 714370.
42. Liang, R. and S. Ghaffari, *Stem cells, redox signaling, and stem cell aging.* Antioxid Redox Signal, 2014. **20**(12): p. 1902-16.
43. Fu, X.J., et al., *NADPH oxidase 1 and its derived reactive oxygen species mediated tissue injury and repair.* Oxid Med Cell Longev, 2014. **2014**: p. 282854.
44. Taylor-Fishwick, D.A., *NOX, NOX Who is There? The Contribution of NADPH Oxidase One to Beta Cell Dysfunction.* Front Endocrinol (Lausanne), 2013. **4**: p. 40.
45. Santabarbara-Ruiz, P., et al., *Ask1 and Akt act synergistically to promote ROS-dependent regeneration in Drosophila.* PLoS Genet, 2019. **15**(1): p. e1007926.

46. Bausek, N., *JAK-STAT signaling in stem cells and their niches in Drosophila.* JAKSTAT, 2013. **2**(3): p. e25686.
47. Gonczy, P., E. Matunis, and S. DiNardo, *bag-of-marbles and benign gonial cell neoplasm act in the germline to restrict proliferation during Drosophila spermatogenesis.* Development, 1997. **124**(21): p. 4361-71.
48. Butturini, E., et al., *S-Glutathionylation at Cys328 and Cys542 impairs STAT3 phosphorylation.* ACS Chem Biol, 2014. **9**(8): p. 1885-93.
49. Xiong, Y., et al., *S-glutathionylation: from molecular mechanisms to health outcomes.* Antioxid Redox Signal, 2011. **15**(1): p. 233-70.
50. DeGennaro, M., et al., *Peroxiredoxin stabilization of DE-cadherin promotes primordial germ cell adhesion.* Dev Cell, 2011. **20**(2): p. 233-43.
51. Karsten, P., S. Hader, and M.P. Zeidler, *Cloning and expression of Drosophila SOCS36E and its potential regulation by the JAK/STAT pathway.* Mech Dev, 2002. **117**(1-2): p. 343-6.
52. Richmond, C.A., et al., *JAK/STAT-1 Signaling Is Required for Reserve Intestinal Stem Cell Activation during Intestinal Regeneration Following Acute Inflammation.* Stem Cell Reports, 2018. **10**(1): p. 17-26.
53. Leatherman, J.L. and S. Dinardo, *Germline self-renewal requires cyst stem cells and stat regulates niche adhesion in Drosophila testes.* Nat Cell Biol, 2010. **12**(8): p. 806-11.
54. Kiger, A.A., H. White-Cooper, and M.T. Fuller, *Somatic support cells restrict germline stem cell self-renewal and promote differentiation.* Nature, 2000. **407**(6805): p. 750-4.
55. Schulz, C., et al., *Signaling from germ cells mediated by the rhomboid homolog stet organizes encapsulation by somatic support cells.* Development, 2002. **129**(19): p. 4523-34.
56. Kalamakis, G., et al., *Quiescence Modulates Stem Cell Maintenance and Regenerative Capacity in the Aging Brain.* Cell, 2019. **176**(6): p. 1407-1419 e14.
57. Snoeck, H.W., *Can Metabolic Mechanisms of Stem Cell Maintenance Explain Aging and the Immortal Germline?* Cell Stem Cell, 2015. **16**(6): p. 582-4.

Figure Legends

Figure 1. Mitochondrial Distribution and Redox Profile of GSCs and CySCs in Adult *Drosophila* Testes

(A) Schematic representation of adult *Drosophila* testicular niche showing arrangement of different stem cell populations (GSC – Germinal Stem Cell, CySC – Cystic Stem Cell). (B-E) Differential distribution of mitochondria labelled with ATP5A (green) in Vasa$^+$ GSCs and Tj$^+$ CySCs of wild-type fly testis; B# shows digitally zoomed image of the dotted area. (F) Relative mitochondria density profile of GSCs and CySCs

denoted through cooccurrence of ATP5A with Tj or Vasa. A.U. - arbitrary units. (G-P) Redox profiling of testicular stem cell niche using *gstD1*-GFP as intrinsic ROS reporter in control (G-K) and *Tj-Gal4* driven *Sod1RNAi (Sod1i)* testis (L-P). (Q) Gaussian distribution curve for the variations in *gstD1*-GFP fluorescence at CySC-GSC intersection region (inset) in *Tj-Gal4* control and *Sod1i* testis. (R) Quantification of mean *gstD1*-GFP fluorescence intensity (MFI) upon Sod1 knockdown represented as fold change over control. Data denotes mean ± s.e.m, n = 25 (S). Colocalization intensity between Vasa and *gstD1*-GFP expressed through Manders' co-localization coefficient (MCC) among control and *Sod1i* cells (G). Controls are the indicated driver line crossed with *Oregon R*$^{+}$. Scale bar - 10 μm. See also Figure S1.

Figure 2. Redox disequilibrium in Cyst stem cell lineage deregulates early CySCs and decreases the GSC number

(A-B) Distribution of Tj^{+} CySC/early cyst cell around the hub (FasIII) in control and driven *Sod1RNAi* testis. (C-D) Represents the rosette arrangement of Vasa^{+} GSCs flanking the hub. The digitally magnified region around the hub (dotted line) as seen in control (C#) and *Sod1RNAi* (D#). (E-G) Mean number of Tj^{+} cells, Zfh1^{+} early CySCs and GSCs in control and *Sod1RNAi* lines shown as mean ± s.e.m, n = 10. (H) Construct design of the FUCCI reporter line for tracking the cell cycle stages in *Drosophila* tissues, containing degrons of Cyclin B and E2F1 proteins fused with RFP or GFP. G1, S and G2/M is represented by GFP^{+}, RFP^{+} and dual labelled cells respectively. (I-J) Comparative changes in the total cell population (I) or Zfh1^{+} cells (J) present in G1, S and G2/M phase at the niche zone between control and *Tj>Sod1i*. Data points denotes mean ± s.e.m, n = 10. (K-X) Representative images showing variations in Zfh1^{+} cells present in different phases of cell cycle among control (K-Q) and experimental flies (R-X). (O, V) shows co-localization of Zfh1 with S-phase cell. Scale bar - 10 μm. See also Figure S2.

Figure 3. ROS imbalance in CySCs promotes differentiation of both GSCs and CySCs

(A-D) Number of early CySCs (Zfh1$^+$) (A'-B'), late differentiating cyst cells (Eya$^+$) (A-B) and Zfh1, Eya co-expressing population were imaged (A"-B"), represented schematically (C) and quantified with respect to control and *Sod1RNAi* lines (D). Data points represent mean ± s.e.m, n = 10. (E-F) The effect of Sod1 depletion in CySCs on the differentiation status of GSCs as observed using *Bam-GFP* reporter line. (G) The relative distance of the differentiation initiation zone (Bam$^+$) from the hub (red) in control and *Sod1i* testis shown as mean ± s.e.m, n = 10. (H-J) The shape and size of the spectrosomes marked with α-spectrin (green) were imaged (I"-J") and quantified for their distance from the hub (marked with asterisk) (H), n = 10. Branched fusome marks differentiating populations (I'-J'). (K-L) Comparative staining of CySC-GSC contacts through adherens junction using E-cadherin (monochrome/green). Dotted area near the hub has been expanded as inset to show loss of E-cadherin network. (M) 3D surface intensity histogram for E-cadherin expression near the hub. (N-O) Fold change in expression of Stat dependent transcripts Socs36E (N) and Ptp61F (O) among control and *Sod1i* niche. Data is shown as mean ± s.e.m, n = 3. Scale bar - 10 *μ*m. See also Figure S3.

Figure 4. Altered CySC redox state disrupted EGFR response.

(A-D) The expression of cell polarity marker Dlg (red) in control and *Sod1i* stem-cell niche was observed (A"-B"), mean florescence intensity (MFI) corresponding to Dlg levels was quantified, n = 75 (C) and the relative spread of the Dlg$^+$ cells irrespective of their expression state was calculated, n = 10 (D). (E) The pErk expression levels at the testicular tip region independent of the cell type, n = 200. (F) Segregated pErk expression patterns in CySCs near the hub and differentiating cyst cells (CC), mean ± s.e.m, n = 200. (G-H) Representative image showing pErk distribution parallelly with Tj$^+$ cells and its expression pattern through Fire LUT (G"-H"). Scale bar - 10 *μ*m. (I-J) The escalation of high pErk regions denoting the differentiation zone (dotted line) was estimated (I) and their distance from the hub was measured (J).

Figure 5. Activated PI3K/Tor associated with early differentiating CySCs.

(A-C) Activation of PI3K/Tor in somatic lineage was adjudged through reporter p4E-BP in *Tj>Sod1i* (A'''-B''') and levels of the active form was quantified (C), MFI – mean fluorescence intensity shown as mean ± s.e.m, n = 40. (D-E) Induction of Akt (D) and Cyclin D (E) in *Sod1i* represented as fold change over controls by mean ± s.e.m, n = 3. (F-M) The number of Tj^+ (F) and $Vasa^+$ (G) cells across control, *Sod1i* and *Sod1i/PI3K*^{DN} (dominant negative allele) depicted as mean ± s.e.m, n = 10. Representative images showing distribution of Tj (I''-J'') and Vasa (L'-M') labelled cells in different genotypes. Scale bar - 10 μm.

Figure 1

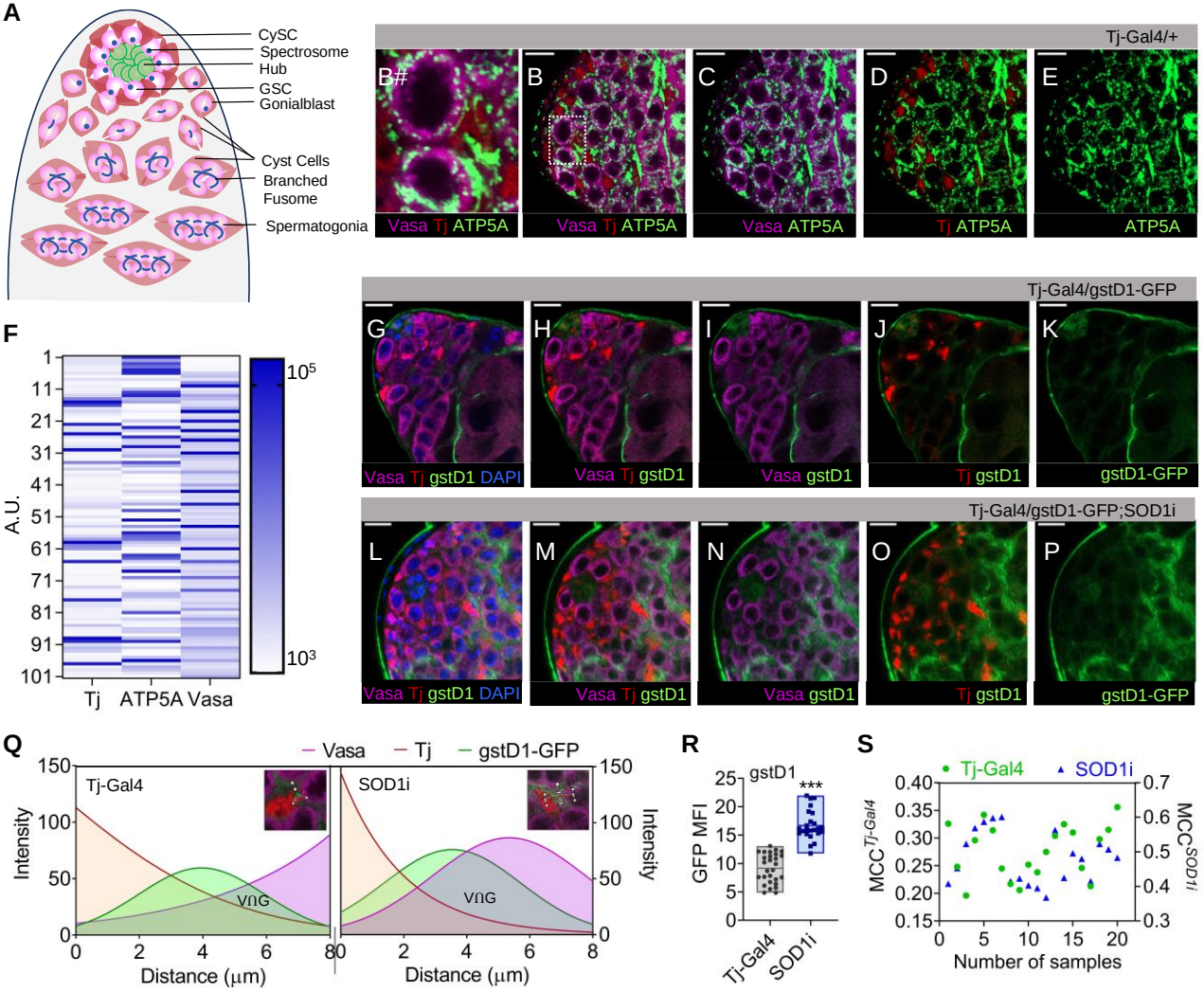
A
CySC
Spectrosome
Hub
GSC
Gonialblast
Cyst Cells
Branched Fusome
Spermatogonia
Tj-Gal4/+
B#
B
C
D
E
Vasa Tj ATP5A
Vasa Tj ATP5A
Vasa ATP5A
Tj ATP5A
ATP5A
Tj-Gal4/gstD1-GFP
G
H
I
J
K
Vasa Tj gstD1 DAPI
Vasa Tj gstD1
Vasa gstD1
Tj gstD1
gstD1-GFP
Tj-Gal4/gstD1-GFP;SOD1i
L
M
N
O
P
Vasa Tj gstD1 DAPI
Vasa Tj gstD1
Vasa gstD1
Tj gstD1
gstD1-GFP
F
A.U.
Tj
ATP5A
Vasa
Q
Vasa
Tj
gstD1-GFP
Tj-Gal4
SOD1i
Intensity
Distance (μm)
R
gstD1
GFP MFI
Tj-Gal4
SOD1i
S
Tj-Gal4
SOD1i
Number of samples

Figure 2

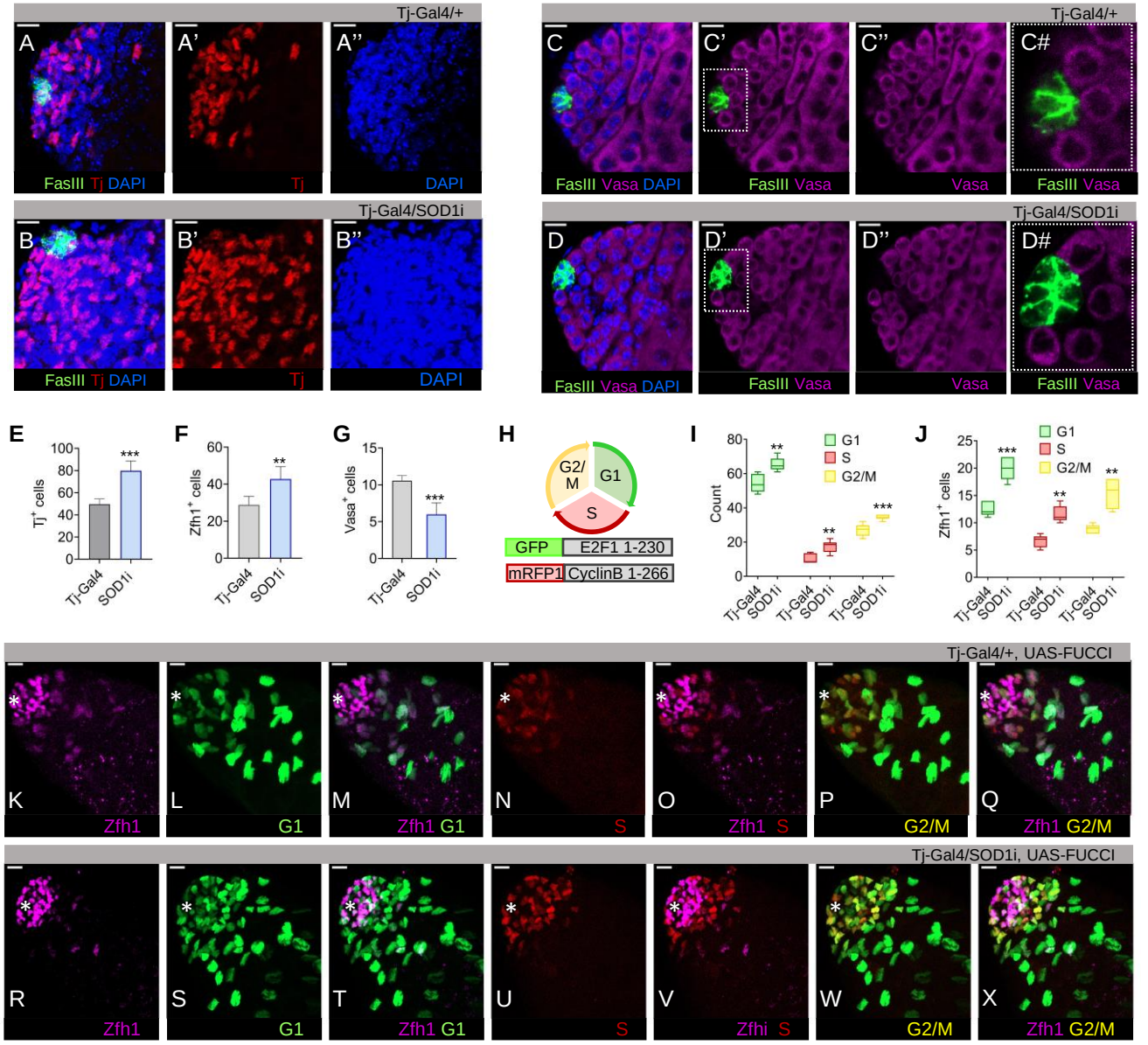
Tj-Gal4/+
A
A'
A''
FasIII Tj DAPI
Tj
DAPI
Tj-Gal4/SOD1i
B
B'
B''
FasIII Tj DAPI
Tj
DAPI
Tj-Gal4/+
C
C'
C''
C#
FasIII Vasa DAPI
FasIII Vasa
Vasa
FasIII Vasa
Tj-Gal4/SOD1i
D
D'
D''
D#
FasIII Vasa DAPI
FasIII Vasa
Vasa
FasIII Vasa
E
Tj+ cells
Tj-Gal4
SOD1i
F
Zfh1+ cells
G
Vasa+ cells
H
G2/M
G1
S
GFP
E2F1 1-230
mRFP1
CyclinB 1-266
I
Count
G1
S
G2/M
J
Zfh1+ cells
Tj-Gal4/+, UAS-FUCCI
K
Zfh1
L
G1
M
Zfh1 G1
N
S
O
Zfh1 S
P
G2/M
Q
Zfh1 G2/M
Tj-Gal4/SOD1i, UAS-FUCCI
R
Zfh1
S
G1
T
Zfh1 G1
U
S
V
Zfhi S
W
G2/M
X
Zfh1 G2/M

Figure 3

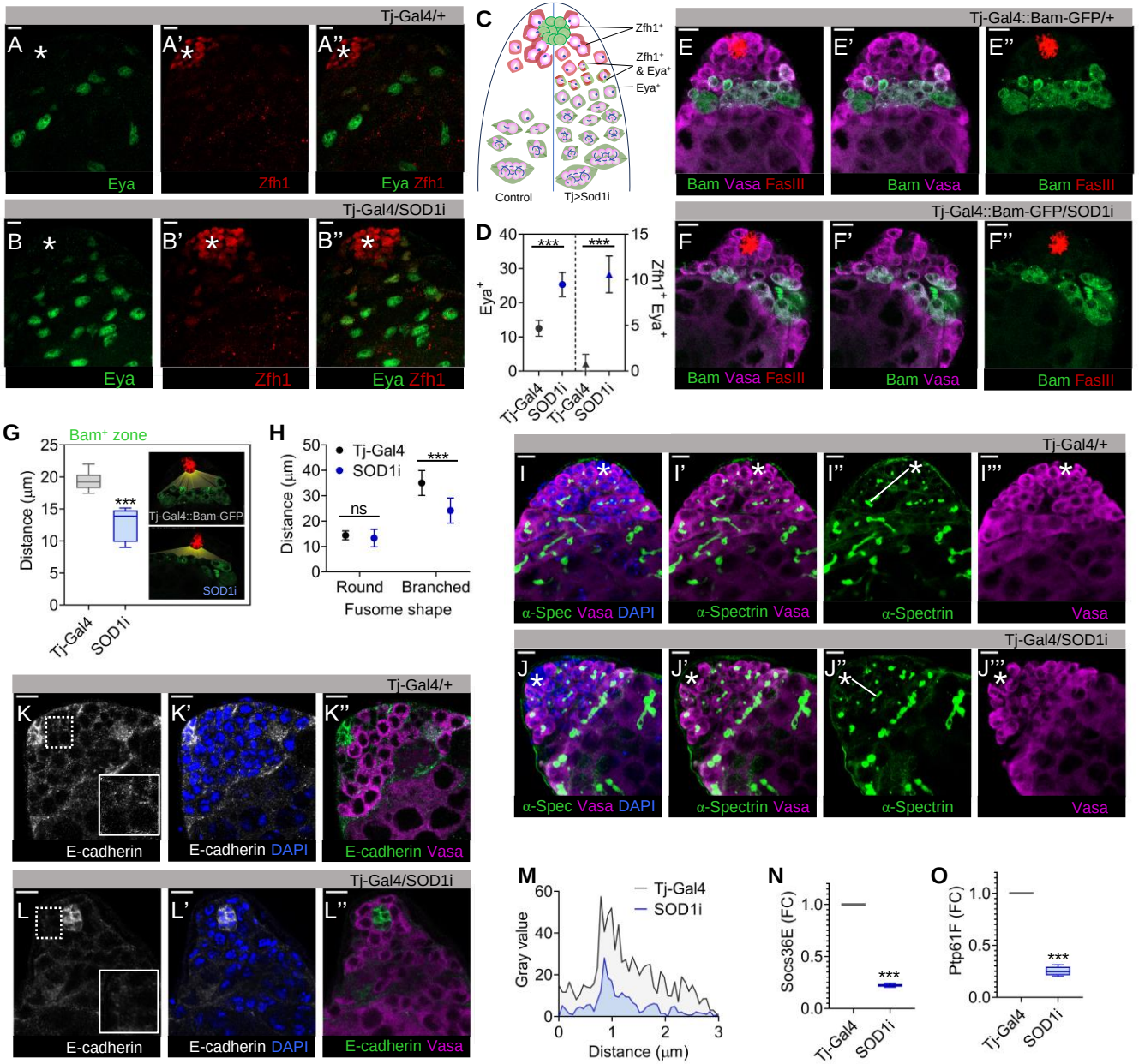
Tj-Gal4/+
A
A'
A''
Eya
Zfh1
Eya Zfh1
Tj-Gal4/SOD1i
B
B'
B''
Eya
Zfh1
Eya Zfh1
C
Zfh1+
Zfh1+ & Eya+
Eya+
Control
Tj>Sod1i
D
Eya+
Zfh1+ Eya+
***
Tj-Gal4
SOD1i
Tj-Gal4::Bam-GFP/+
E
E'
E''
Bam Vasa FasIII
Bam Vasa
Bam FasIII
Tj-Gal4::Bam-GFP/SOD1i
F
F'
F''
Bam Vasa FasIII
Bam Vasa
Bam FasIII
G
Bam+ zone
Distance (μm)
Tj-Gal4::Bam-GFP
SOD1i
H
Tj-Gal4
SOD1i
ns
Round
Branched
Fusome shape
Tj-Gal4/+
I
I'
I''
I'''
α-Spec Vasa DAPI
α-Spectrin Vasa
α-Spectrin
Vasa
Tj-Gal4/SOD1i
J
J'
J''
J'''
α-Spec Vasa DAPI
α-Spectrin Vasa
α-Spectrin
Vasa
Tj-Gal4/+
K
K'
K''
E-cadherin
E-cadherin DAPI
E-cadherin Vasa
Tj-Gal4/SOD1i
L
L'
L''
E-cadherin
E-cadherin DAPI
E-cadherin Vasa
M
Tj-Gal4
SOD1i
Gray value
Distance (μm)
N
Socs36E (FC)
Tj-Gal4
SOD1i
O
Ptp61F (FC)
Tj-Gal4
SOD1i

Figure 4

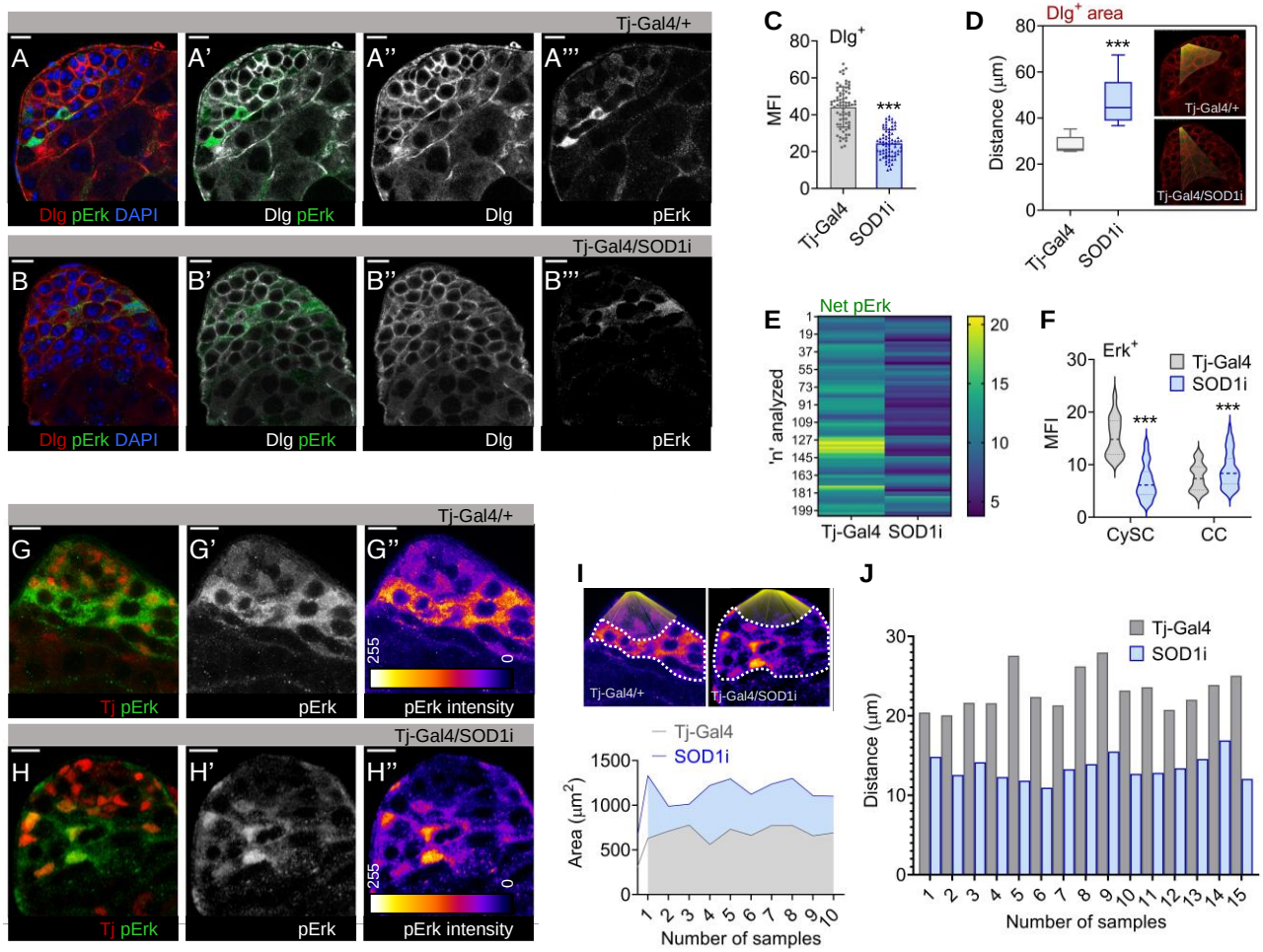
Tj-Gal4/+
A
A'
A''
A'''
Dlg pErk DAPI
Dlg pErk
Dlg
pErk
Tj-Gal4/SOD1i
B
B'
B''
B'''
Dlg pErk DAPI
Dlg pErk
Dlg
pErk
C
Dlg+
MFI
***
Tj-Gal4
SOD1i
D
Dlg+ area
Distance (µm)
***
Tj-Gal4/+
Tj-Gal4/SOD1i
Tj-Gal4
SOD1i
E
Net pErk
'n' analyzed
Tj-Gal4 SOD1i
F
Erk+
MFI
Tj-Gal4
SOD1i
***
***
CySC
CC
Tj-Gal4/+
G
G'
G''
Tj pErk
pErk
pErk intensity
255
0
Tj-Gal4/SOD1i
H
H'
H''
Tj pErk
pErk
pErk intensity
255
0
I
Tj-Gal4/+
Tj-Gal4/SOD1i
Tj-Gal4
SOD1i
Area (µm2)
Number of samples
J
Tj-Gal4
SOD1i
Distance (µm)
Number of samples

Figure 5

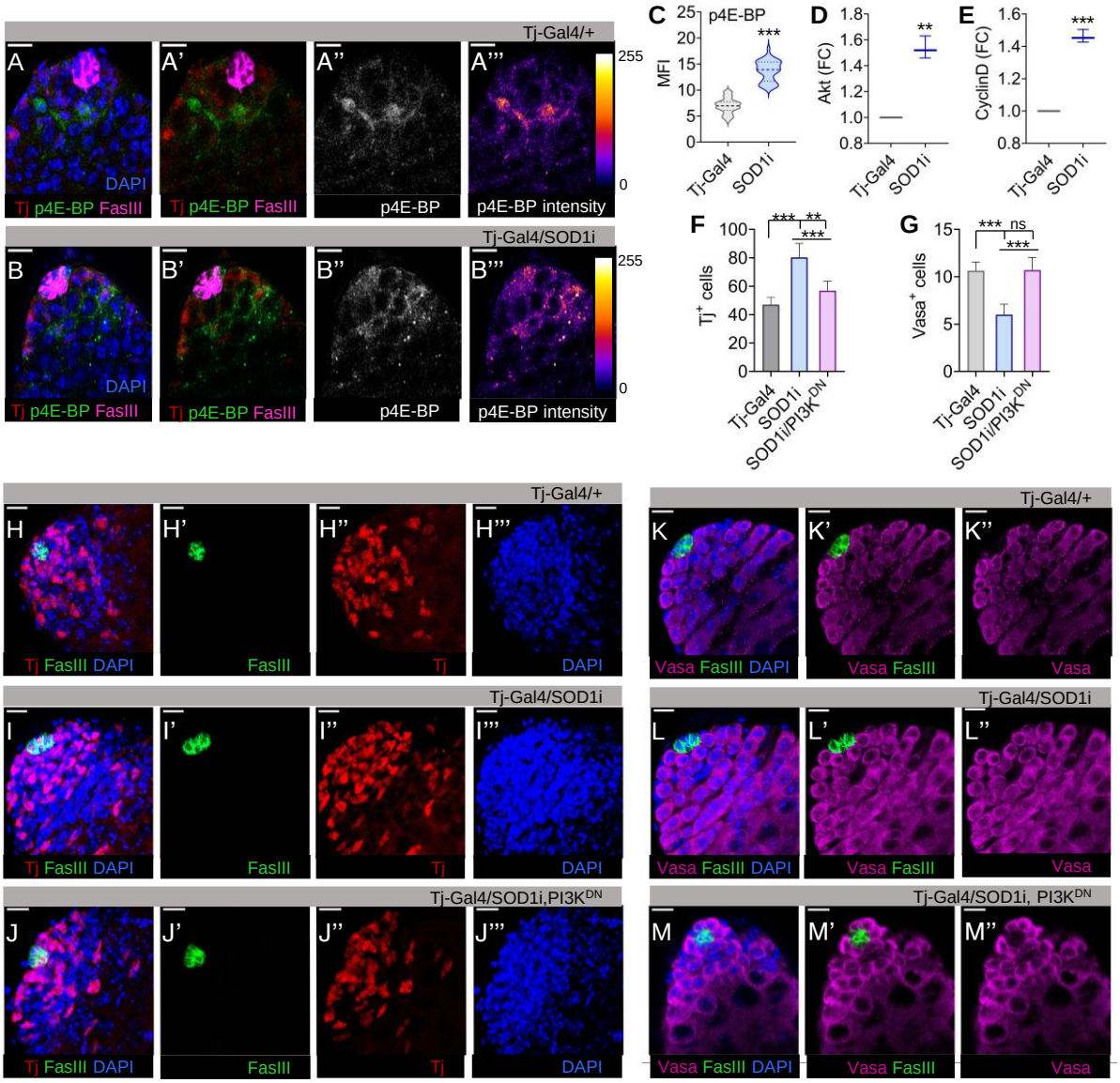
Tj-Gal4/+
A
A'
A''
A'''
DAPI
Tj p4E-BP FasIII
Tj p4E-BP FasIII
p4E-BP
p4E-BP intensity
255
0
Tj-Gal4/SOD1i
B
B'
B''
B'''
DAPI
Tj p4E-BP FasIII
Tj p4E-BP FasIII
p4E-BP
p4E-BP intensity
255
0
C
p4E-BP
MFI
***
Tj-Gal4
SOD1i
D
Akt (FC)
**
Tj-Gal4
SOD1i
E
CyclinD (FC)
***
Tj-Gal4
SOD1i
F
Tj+ cells
***
**
***
Tj-Gal4
SOD1i
SOD1i/PI3K DN
G
Vasa+ cells
***
ns
***
Tj-Gal4
SOD1i
SOD1i/PI3K DN
Tj-Gal4/+
H
H'
H''
H'''
Tj FasIII DAPI
FasIII
Tj
DAPI
Tj-Gal4/+
K
K'
K''
Vasa FasIII DAPI
Vasa FasIII
Vasa
Tj-Gal4/SOD1i
I
I'
I''
I'''
Tj FasIII DAPI
FasIII
Tj
DAPI
Tj-Gal4/SOD1i
L
L'
L''
Vasa FasIII DAPI
Vasa FasIII
Vasa
Tj-Gal4/SOD1i,PI3K DN
J
J'
J''
J'''
Tj FasIII DAPI
FasIII
Tj
DAPI
Tj-Gal4/SOD1i, PI3K DN
M
M'
M''
Vasa FasIII DAPI
Vasa FasIII
Vasa